Boussinesq modelling of wave-induced horizontal particle velocities

Bosboom, J.; Klopman, G.; Roelvink, J. A.; Battjes, J. A.

DOI
10.1016/S0378-3839(97)81748-6

Publication date
1997

Document Version
Final published version

Published in
Coastal Engineering

ELSEVIER

Coastal Engineering 32 (1997) 163–180

COASTAL ENGINEERING

Boussinesq modelling of wave-induced horizontal particle velocities

J. Bosboom [a,b,*], G. Klopman [a,b], J.A. Roelvink [a,b], J.A. Battjes [b]

[a] *Delft Hydraulics, P.O. Box 177, 2600 MH Delft, Netherlands*

[b] *Netherlands Center for Coastal Research, Department of Civil Engineering, Delft University of Technology, Stevinweg 1, P.O. Box 5048, 2600 GA Delft, Netherlands*

Received 17 June 1996; accepted 19 June 1997

Abstract

A frequency–domain Boussinesq model with good linear shoaling, improved linear dispersion characteristics and a dissipation formulation to account for wave breaking is extended to include the computation of the vertical structure of the horizontal velocity. The extended model is used to predict bottom velocities and resulting velocity variance and skewness in (partially) breaking irregular waves. The comparison of measured and computed velocity moments indicates that for moderately long waves the spectral Boussinesq model can be successfully used for sediment transport purposes. For shorter waves the crest velocity values of the higher waves are significantly underestimated, and as a result the velocity skewness as well. © 1997 Elsevier Science B.V.

Keywords: Boussinesq models; Particle velocities; Wave kinematics; Surf zone; Wave breaking; Coastal hydrodynamics

1. Introduction

The development of numerical models capable of reproducing the hydrodynamics field in the shoaling region and the surf zone is of particular interest to coastal morphological problems. From an evaluation of sediment transport formulations (Bailard, 1981; Roelvink and Stive, 1989), it appears that the third and fourth oscillatory velocity moments ($\langle u^3 \rangle$ and $\langle |u|^3 u \rangle$ respectively), are the most important parameters in determining the magnitude of the wave-induced sediment transport. These moments are

* Corresponding author. Fax: +31-15-2858582; e-mail: judith.bosboom@wldelft.nl.

PII S0378-3839(97)00023-9

non-zero only for asymmetric (non-linear) motions such as occur in shallow water. The generation of free and bound sub- and super-harmonics in shallow water leads to asymmetries of the free-surface and velocity time series about both the horizontal and vertical axis. Since Boussinesq equations include non-linearity, they are suitable for the description of these asymmetry effects. Moreover, they require relatively little computational effort, since the equations are integrated over the water depth and therefore only formulated in the horizontal space.

Boussinesq equations, describing relatively long, small amplitude waves propagating in water of varying depth, are derived from the potential flow equations assuming that the depth-dependence of the velocity field is weak. The vertical momentum equation is eliminated while ignoring the non-linear vertical acceleration. This implies that a parabolic vertical structure of the horizontal velocities is assumed. The equations are stated in the surface elevation and one single horizontal velocity variable, the so-called computational velocity. Many different forms of Boussinesq equations exist, which differ in frequency–dispersion and shoaling characteristics as well as in the computational velocity variable. Because of the water-depth restriction of Boussinesq equations, efforts have recently been spent on improving the linear frequency dispersion with respect to the conventional Boussinesq equations. Reference is made to Witting (1984), Madsen et al. (1991), Madsen and Sørensen (1992), Nwogu (1993), Dingemans (1994, 1997) and Schröter (1995). Improvement of the frequency dispersion typically leads to another form of the equations in which different third derivative frequency–dispersion terms occur.

The validation of Boussinesq models has been primarily focused on the surface elevations. Madsen and Sørensen (1992) suggested time-domain equations valid for a slowly-varying bathymetry in which the frequency dispersion was improved with respect to the conventional Boussinesq equations. They verified the numerical model with respect to shoaling and refraction–diffraction in deep and shallow water. Beji and Battjes (1994) presented a one-dimensional time-domain model based on a form of the equations derived from Madsen et al. (1991). Comparisons for non-breaking waves showed good agreement between the numerical results and measurements obtained from experiments in a wave channel with a submerged trapezoidal bar.

Besides these time-domain formulations, frequency–domain formulations have been developed leading to coupled evolution equations for slowly-varying complex Fourier amplitudes. Evolution equations have been presented by numerous authors on the basis of various forms of Boussinesq-type equations. Freilich and Guza (1984) were the first to consider evolution equations valid for a mildly sloping bottom and non-breaking waves. They made the assumption that bound wave energy could be neglected and that substantial carrying wave energy should be present at all frequencies at all times. Applications and verifications of their model (Elgar and Guza, 1985, 1986; Elgar et al., 1990; Freilich et al., 1990) showed good agreement between measured and computed spectral properties in the shoaling region, i.e. outside the breaker zone.

Frequency–domain versions of equations with improved frequency dispersion (Madsen and Sørensen, 1992) and without the assumptions made by Freilich and Guza (1984) were presented by Madsen and Sørensen (1993). They concluded that the agreement between the spectral evolution equations and the time–domain counterpart is most

satisfactory, except for the peak values of the highest waves which are underestimated by the spectral evolution equations.

Attempts have also been made to include a formulation for wave breaking in Boussinesq equations to extend their applicability to the surf zone. Deigaard (1989) suggested the concept of surface rollers to describe the breaking mechanism in Boussinesq equations. A modification of this approach was incorporated in conventional time–domain Boussinesq equations by Schäffer et al. (1993). Eldeberky and Battjes (1996) supplemented the evolution equations of Madsen and Sørensen (1993) with a spectral breaking term which accounts for the energy dissipation due to wave breaking (see, also, Battjes et al., 1993).

The knowledge about the capability of Boussinesq models in reproducing the velocity field is very limited. Recently, efforts have been spent on testing Boussinesq models against velocity data. Both Brocchini et al. (1992) and Quinn et al. (1994) considered velocity data for waves breaking partially on a gently sloping beach. The velocity data were compared with results obtained with amongst others a model based on conventional Boussinesq equations. The description of the breaking process was based on the roller concept (Schäffer et al., 1993). Brocchini et al. (1992) worked out comparisons on velocity data, both on depth-averaged horizontal velocities and on vertical profiles related to the depth-averaged velocity through a parabolic expression. It was found that the Boussinesq model gave a systematic overestimation of the velocity. A more extensive comparison was carried out by Quinn et al. (1994). They found that the computed depth-averaged velocity components slightly exceeded the measured values. Further, it was concluded that the reconstruction of the velocity field by imposing a parabolic profile is in good agreement with measured vertical profiles, especially in the near-bed zone (see, also, Bosboom et al., 1996). The parabolic profile however, was seen to exceed the measured values near the surface, particularly in the crest locations. Using the model of Freilich and Guza (1984), Elgar et al. (1990) found good agreement between predicted and measured second and third moments of horizontal velocity and acceleration fields in the shoaling region.

The purpose of this paper is to validate the Boussinesq modelling of horizontal velocities under (breaking) waves, especially in the near-bed zone, using a frequency–domain model extended with breaking dissipation (Eldeberky and Battjes, 1996). This model is based on time–domain equations with good shoaling behavior and improved frequency dispersion (Madsen and Sørensen, 1992).

We present the extension of the spectral model, which is stated in terms of the surface elevation only, with the computation of the depth-averaged velocity and, consequently, the vertical profile of the horizontal velocity by imposing a parabolic profile, as is consistent with the Bousssinesq approximation. The parabolic profile to obtain the horizontal velocity as a function of the depth was found to yield realistic results (Quinn et al., 1994; Bosboom et al., 1996), especially in the near-bed zone where we will focus on in this paper. The model is verified through comparisons with measured bottom velocities in laboratory measurements of irregular waves (partially) breaking on a sandy beach. The comparison between measurements and computations is performed on velocity variance and skewness, the latter being the most important variable in determining the magnitude of the net bed-load transport rate.

The organization of this paper is as follows. Section 2 recapitulates the spectral model with breaking dissipation and presents the extension to compute the vertical profile of the horizontal velocity. Further, this section deals with the discretization of the model equations. Verification of the spectral velocity modelling is presented in Section 3. Finally, in Section 4 a summary and conclusions are given.

2. Spectral Boussinesq model and flow field reconstruction

2.1. Governing equations

A frequency–domain approach based on evolution equations and Fourier series approximations is used. Assuming slowly-varying uni-directional wave propagation, evolution equations for the complex amplitudes were derived by Madsen and Sørensen (1993) and supplemented with a breaking formulation by Eldeberky and Battjes (1996). In this section the extension of this spectral model with the computation of the vertical profile of the horizontal velocity is presented.

Starting point of the derivation of the spectral equations were time–domain Boussinesq equations stated in terms of the volume flux per unit width q (Madsen and Sørensen, 1992). The Boussinesq approximation is valid for weakly non-linear moderately long waves:

$$\varepsilon = \frac{a}{h} \ll 1, \quad \text{non-linearity parameter,}$$

$$\mu = \left(\frac{h}{L}\right)^2 \ll 1, \quad \text{dispersion parameter,}$$

$$\frac{\varepsilon}{\mu} = O(1).$$

where a is the wave amplitude, h is the undisturbed water depth and L is the wave length. The assumption that $\mu \ll 1$ implies that the bottom slope $|\mathrm{d}h/\mathrm{d}x| \leq \mu^{1/2}$ (Dingemans, 1994, 1997). Madsen and Sørensen (1992) further assume a slowly-varying bathymetry ($|\mathrm{d}h/\mathrm{d}x| \ll \mu^{1/2}$); bottom-slope squared and bottom-curvature terms are neglected in the equations. Their equations read:

$$\zeta_t + g_x = 0, \tag{1a}$$

$$q_t + \left(\frac{q^2}{h+\zeta}\right)_x + g(h+\zeta)\zeta_x = \left(\tfrac{1}{3} + b\right)h^2 q_{txx} + bgh^3\zeta_{xxx} + hh_x\left[\tfrac{1}{3}q_{tx} + 2bgh\zeta_{xx}\right]. \tag{1b}$$

Here the subscripts denote partial differentiation with respect to the indicated indices, ζ is the free-surface elevation, q is the depth-integrated horizontal velocity (or the volume flux per unit width), g is the acceleration due to gravity and b is a fitting parameter for obtaining the best agreement with the frequency dispersion according to Stokes' first

order theory. For $b = 1/15$ the phase celerity errors are minimized over the whole range of kh (see Madsen and Sørensen, 1992; Dingemans, 1994, 1997).

In deriving the frequency–domain counterpart of Eqs. (1a) and (1b), Madsen and Sørensen (1993) formulated solutions for the free-surface elevation in terms of Fourier series with spatially varying coefficients:

$$\zeta(x, t) = \sum_{p=-\infty}^{\infty} A_p(x) \exp\left[\mathrm{i}\left(\omega_p t - \psi_p(x)\right)\right], \tag{2}$$

where p indicates the rank of the harmonic, A_p is the complex Fourier amplitude, ω_p is the angular frequency and $\mathrm{d}\psi_p/\mathrm{d}x = k_p(x)$ is the wave number in the linear approximation, with k_p determined from the linear dispersion relation of the equations. Note that $\omega_{-p} = -\omega_p$, $\psi_{-p} = -\psi_p$, $A_{-p} = A_p^*$ with '*' denoting the complex conjugate. The frequencies are determined by $\omega_p = p\Delta\omega$ where $\Delta\omega$ is the lowest frequency of interest.

A lowest-order estimate of the volume flux per unit width q is obtained by combining the Fourier series expansion for ζ (2) with the continuity Eq. (1a) while neglecting the first derivatives of A_p and k_p:

$$q(x, t) \approx \sum_{p=-\infty}^{\infty} \frac{\omega_p}{k_p} A_p(x) \exp\left[\mathrm{i}\left(\omega_p t - \psi_p(x)\right)\right]. \tag{3}$$

Inserting Eqs. (2) and (3) in the time–domain equations yields after some algebraic manipulations first-order evolution equations for the complex Fourier amplitudes. In this procedure, first derivatives of A_p, k_p and h are assumed to be small and products of derivatives and higher derivatives of these quantities are neglected in the formulation.

Madsen and Sørensen (1993) found that the agreement between the surface elevations predicted by the time–domain equations and the evolution equations is most satisfactory. The only discrepancy is found in the highest waves where the evolution equations underestimate the peak values.

Eldeberky and Battjes (1996) supplemented the evolution equations with a semi-empirical dissipation formulation for the total energy loss due to breaking which reduces the spectral amplitudes in the same proportion without affecting the spectral shape. The evolution equations then read, with p covering the interval from $p = 1$ to ∞,

$$\frac{\mathrm{d}A_p}{\mathrm{d}x} = -\beta_2 \frac{h_x}{h} A_p - \mathrm{i}2g\left(F_p^+ + F_p^-\right) - \frac{1}{2}\frac{D}{F} A_p, \tag{4}$$

where the first term in the right-hand side of Eq. (4) represents linear shoaling, the second and the third term represent the triad sum and difference interactions respectively and the last term is the dissipation term representing the contribution due to wave breaking. Here F is the total local rate of energy flux per unit width and D is the total local rate of random-wave energy dissipation per unit area due to breaking. The terms F_p^+ and F_p^- are defined by

$$F_p^+ = \sum_{m=1}^{p-1} \frac{\alpha^+}{2\beta_1} A_m A_{p-m} \exp\left[-\mathrm{i}\left(\psi_m + \psi_{p-m} - \psi_p\right)\right],$$

$$F_p^- = \sum_{m=1}^{\infty} \frac{\alpha^-}{\beta_1} A_m^* A_{p+m} \exp\left[-\mathrm{i}\left(\psi_{m+p} - \psi_m - \psi_p\right)\right]. \tag{5}$$

For expressions for the shoaling coefficient β_2 in Eq. (4) and the interaction coefficients β_1, α^+ and α^- in Eq. (5) one is referred to Madsen and Sørensen (1993) and Eldeberky and Battjes (1996). The energy dissipation rate D can be computed using the energy dissipation model of Battjes and Janssen (1978) or comparable methods (e.g., Thornton and Guza, 1983); here we use the model of Battjes and Janssen (1978).

The extended model has been used by Eldeberky and Battjes (1996) to predict surface elevations and surface elevation spectra. The results showed encouraging agreement with observed surface elevation time series as well as spectra. It was found that the effects of wave breaking were adequately described by the reduction of the complex amplitudes A_p with a frequency-independent real factor; there is no need of a phase shift induced by wave breaking.

Since we are interested in horizontal velocity values at various heights, an expression must be found for the horizontal velocity as a function of the depth in terms of the complex Fourier amplitudes A_p.

In the linear approximation, the depth-averaged velocity is determined from the lowest-order approximation of the volume flux q (Eq. (3)) as follows:

$$\bar{u}(x, t) \approx \frac{q}{h} \approx \sum_{p=-\infty}^{\infty} \frac{\omega_p}{k_p h} A_p(x) \exp\left[\mathrm{i}\left(\omega_p t - \psi_p(x)\right)\right]. \tag{6}$$

Note that in this way only the purely oscillating part of the horizontal velocity is predicted by the model; the time-averaged component of the velocity is eliminated upon linearization.

In order to compute the horizontal velocity profile as a function of the depth, a parabolic profile is imposed. As a first approximation we use the parabolic profile for the constant depth situation:

$$u(x, z, t) = \bar{u} - \left[\tfrac{1}{3}h^2 + zh + \tfrac{1}{2}z^2\right]\bar{u}_{xx}, \tag{7}$$

where $z = 0$ corresponds to the undisturbed position of the free surface. Substitution of Eq. (6) in Eq. (7) while neglecting all derivatives of A_p, k_p and h, yields the following expression for the horizontal velocity profile in terms of Fourier series:

$$u(x, z, t) = \sum_{p=-\infty}^{\infty} U_p(x, z) \exp\left[\mathrm{i}\left(\omega_p t - \psi_p(x)\right)\right], \tag{8a}$$

with

$$\frac{U_p(x, z)}{A_p(x)} = \frac{\omega_p}{k_p h}\left[1 + k_p^2\left[\frac{1}{3}h^2 + zh + \frac{1}{2}z^2\right]\right]. \tag{8b}$$

2.2. Numerical integration

The evolution equations (Eq. (4)) are first-order ordinary differential equations. They are numerically integrated using a fourth-order Runge–Kutta method. The upwave boundary condition for the integration is a set of complex amplitudes A_p ($p = 1, 2, 3,$

..., P). Those amplitudes can be obtained from measured time records of the surface elevation by the use of a standard fast Fourier transformation algorithm.

The result of the numerical integration is a set of complex amplitudes A_p at each location. The phases of the complex amplitudes, predicted by the evolution equations, only contain the non-linear phase. The linear part of the phase function is computed separately by integrating k_p spatially. The non-linear and linear parts are added in order to obtain the total wave phase.

The numerical model of Eldeberky and Battjes (1996) was extended to compute the complex amplitudes U_p at each output location and at various vertical positions by multiplication of A_p by the expression in the right-hand side of Eq. (8b). The surface elevation and velocity time records can be obtained by post-processing the complex amplitudes by means of an inverse fast Fourier transformation.

3. Verification of the extended model

3.1. Experimental data

The prediction of horizontal velocities and velocity moments was verified against wave channel measurements of irregular (partially) breaking waves propagating over a concave sandy beach. The experiments were carried out within the framework of the EU-sponsored Large Installations plan (Arcilla et al., 1994; Roelvink and Reniers, 1995). Two different experimental data sets (i.e., test 1a and 1c) were used. These two experiments were already used by Eldeberky and Battjes (1996) for the comparison of measured and computed surface elevation time series and spectra.

The incident wave conditions are listed in Table 1, in which T_p is the peak period and H_{m0} the significant wave height. Table 1 also shows the non-linearity parameter $\varepsilon = a/h$ (in which the wave amplitude $a = H_{m0}/2$) and the dispersion parameter $\mu = (h/L)^2$ (in which L is the wave length corresponding to the peak period) at a water depth $h = 4.1$ m.

In the experiments the low-frequency wave channel resonances were prevented by an active wave absorption system at the wave-maker. Surface elevations and velocities were measured at several locations along the wave channel. The velocity measurements were carried out at several distances from the bed. The velocity measurement locations are indicated in Fig. 1, for both experiments. Since the spectral model only predicts the purely oscillating part of the velocity the time-averaged velocity component was filtered from the measured signals.

Table 1
Wave parameters for experiments 1a and 1c

Test	T_p (s)	H_{m0} (m)	ε	μ
1a	4.9	0.9	0.11	0.021
1c	8.0	0.6	0.07	0.007

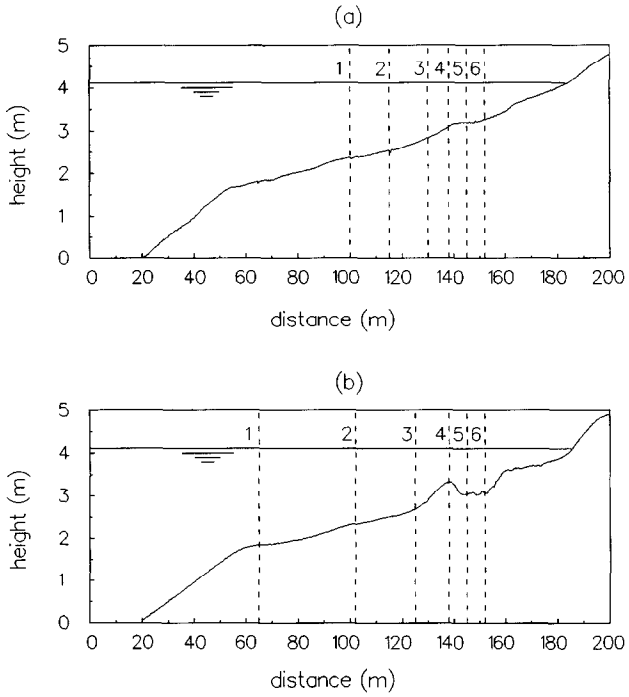

Fig. 1. Bed profile and location of electronic current meters for (a) experiment 1a and (b) experiment 1c (Roelvink and Reniers, 1995).

For experiment 1a, the incident wave conditions are such that the wave breaking is strong. The monotonic sandy beach profile (Fig. 1a) allows for wave breaking to take place over a large distance; the experiments showed a gradual decrease of the significant wave height at distances from 100 m up to about 140 m from the wave board, beyond which the wave breaking gets strong. In experiment 1c on the contrary, a barred beach profile is present (Fig. 1b). The wave breaking is mild and is concentrated behind the bar, the crest of which is located around 138 m.

The upwave boundary conditions used in the numerical computations are obtained from the measured surface elevations at 20 m by the use of a standard FFT algorithm.

3.2. Computational parameters

Besides the bottom geometry and the upwave boundary, the model input comprises the breaking coefficient $\gamma = H_m/h$ in which H_m is the maximum wave height, the bandwidth Δf, the number of frequency components P and the spatial step Δx. The spatial step was chosen $\Delta x = 0.5$ m and the breaking coefficient $\gamma = 0.85$ in accordance with the γ-value used by Eldeberky and Battjes (1996). This value is on the high side to compensate for the use of the mean frequency instead of the more commonly used peak frequency in the formulation of the energy-dissipation rate D.

The sampling rate in the measurements is 10 Hz implying a maximum cut-off frequency in the simulations of 5 Hz. Too large a cut-off frequency however, resulted in extremely noisy velocity signals due to the amplification of higher harmonics in the computation of $\bar{u}_{xx}$ in Eq. (7). This could be avoided by choosing a cut-off frequency of 1 Hz in the simulations, which was still high enough to adequately represent all harmonics. The length of the simulated time record was $T = 2048$ s for both experiments, resulting in a number of frequency components $P = 2048$ and a bandwidth $\Delta f = 4.883 \times 10^{-4}$ Hz.

3.3. Analysis of time-series

In view of the approximately uniform vertical distribution of the horizontal velocity in both experiments, only bottom velocities, measured at 10 cm above the bed, were focused on. The comparison between measurements and computations was carried out on bottom velocity time series, variance and skewness. For experiment 1a, also surface elevation time records will be shown in order to compare the accuracy in predicting the horizontal velocities and the surface elevation.

In computing the variance and skewness of the bottom velocity, it was assumed that the total oscillatory velocity signal u consists of a short wave averaged low-frequency component u_{lo} and a short wave component u_{hi}.

Assuming u_{lo} and u_{hi} to be uncorrelated, the velocity variance is given by:

$$\langle u^2 \rangle = \langle u_{\mathrm{hi}}^2 \rangle + \langle u_{\mathrm{lo}}^2 \rangle, \tag{9a}$$

where the $\langle\ \rangle$ indicate time-averaging over the short wave and wave group scale.

Assuming in addition that $u_{\mathrm{lo}} \ll u_{\mathrm{hi}}$, Roelvink and Stive (1989) demonstrated that the most important contributions of the oscillatory part of the velocity to the velocity skewness are given by:

$$\langle u^3 \rangle = \langle u_{\mathrm{hi}}^3 \rangle + 3\langle u_{\mathrm{hi}}^2 u_{\mathrm{lo}} \rangle + \ldots. \tag{9b}$$

The first term in the right-hand side of Eq. (9b) is related to the short wave asymmetry, whereas the second term is associated with the interaction between the long wave velocity and the slowly-varying short wave velocity variance.

For both the measured and the computed bottom velocity time series, the terms in the left-hand side as well as the right-hand side of Eqs. (9a) and (9b) were calculated using half the peak frequency for the lowest short wave frequency.

3.4. Discussion of results

The comparisons between the predicted and measured results are given in Figs. 2–6. Generally, it was found that the accuracy in predicting the bottom velocity is comparable to the accuracy in predicting the surface elevation; for test 1a, this can be seen by comparing Figs. 2 and 3.

Figs. 2 and 3 demonstrate that in test 1a both the predicted surface elevation time series, which correspond with the results presented in Eldeberky and Battjes (1996), and

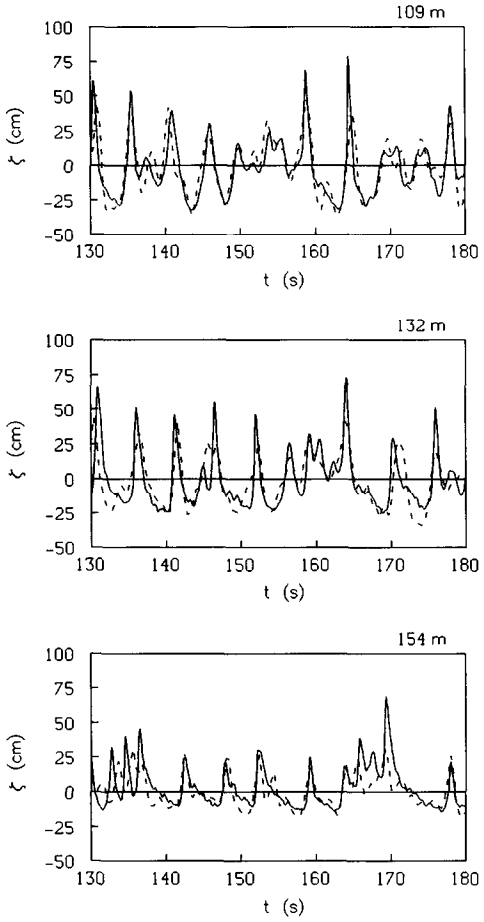

Fig. 2. Comparison of time series of measured (solid line) and computed (dotted line) surface elevations for experiment 1a.

bottom velocity time series underestimate the peak values of the highest waves, resulting in too much symmetry in the computed signals.

Fig. 4 shows that, except for the last station behind the bar, the short wave velocity variance is very well predicted, suggesting that the spectral energy density for the higher frequencies is well reproduced by the model. The model slightly underestimates the total velocity variance for the stations closest to the bar. This can be seen to originate from the inaccurate reproduction of the long wave velocity variance for these stations. It may be that the dissipation due to short wave breaking should not have been applied in this frequency band. Note that Eldeberky and Battjes (1996) on the basis of their results could not draw firm conclusions on whether to apply the breaking dissipation to the low-frequency waves. Another possible explanation might be the presence of a standing low-frequency wave pattern near the beach with a node in the low-frequency surface

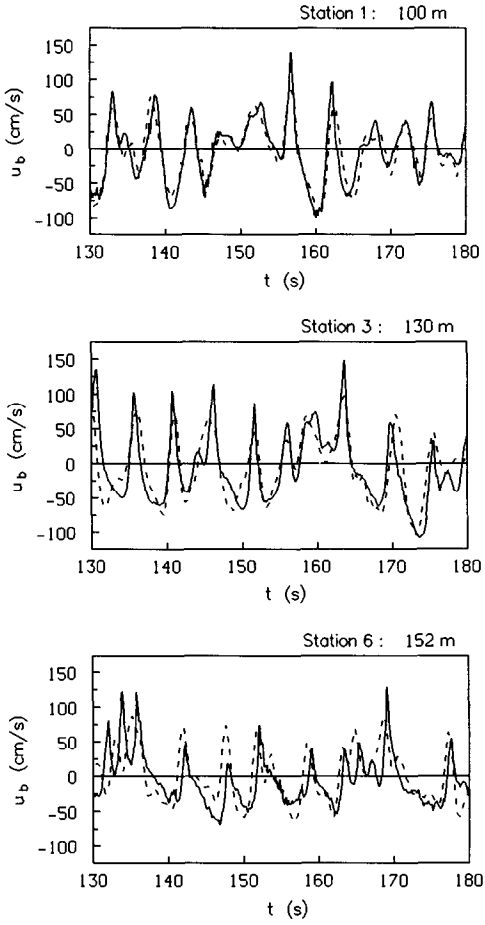

Fig. 3. Comparison of time series of the measured (solid line) and computed (dotted line) bottom velocity for experiment 1a.

elevation and hence large velocity amplitudes around station 5. Standing waves are not reproduced by the model because of the assumption of uni-directional wave propagation.

As a result of the underestimation of the velocity crest values of the highest waves, the velocity skewness (Fig. 4), which can be seen to be dominated by the short wave asymmetry, is largely underestimated by the model. The agreement is reasonable for the last two stations where strong wave breaking occurs. The long wave contribution is predicted rather well. Increasing the maximum frequency and the frequency resolution did not improve the numerical results.

Test 1c shows an encouraging agreement between measured and predicted bottom velocity time series (Fig. 5), variance and skewness (Fig. 6), especially up to the bar crest. In contrast with test 1a, both the peak values and form of the velocity signal are predicted reasonably well. The underestimation of the peak values is less significant than

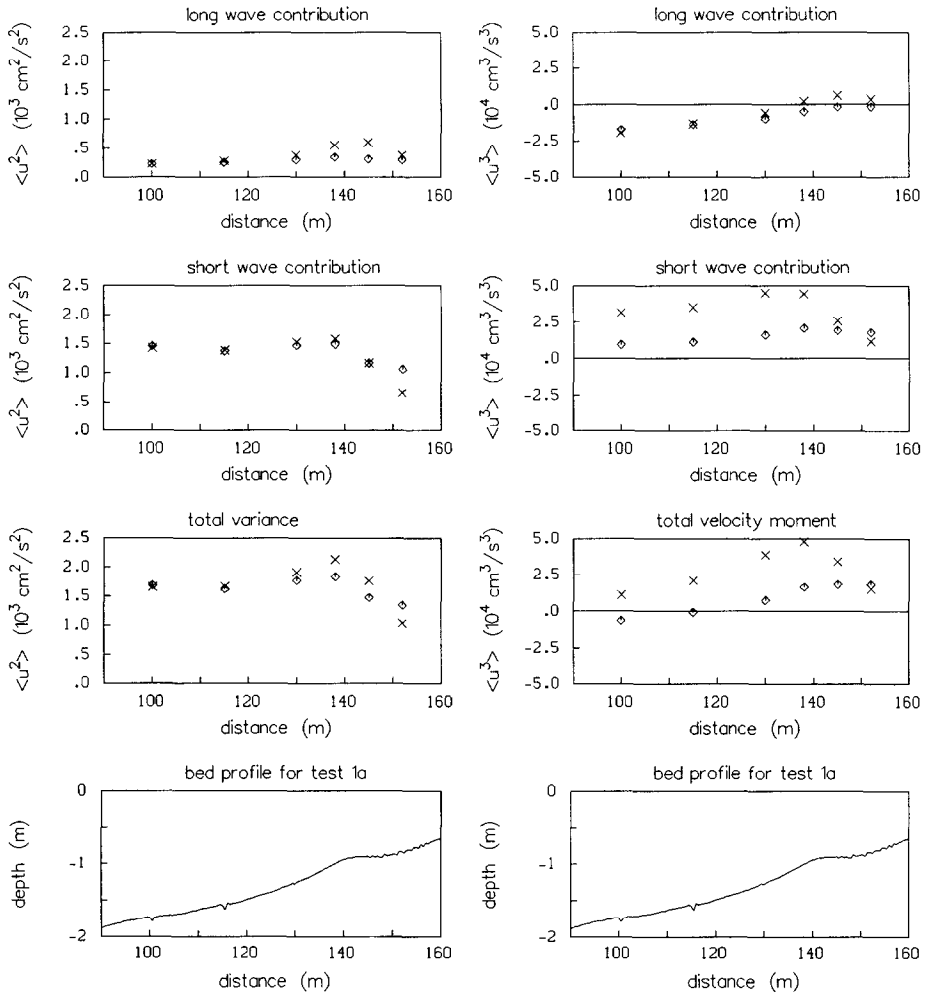

Fig. 4. Comparison of measured (crosses) and computed (diamonds) bottom velocity variance (left) and skewness (right): long wave contribution, short wave contribution and total moment respectively; experiment 1a.

for test 1a. The less good agreement beyond the bar crest, also found by Eldeberky and Battjes (1996) for surface elevation spectra, can possibly be ascribed to the relatively steep bottom beyond the bar crest ($h_x/\mu^{1/2} = 0.52$) which is in contrast with the assumption of slowly-varying bottom ($h_x/\mu^{1/2} \ll 1$).

The velocity variance in test 1c (Fig. 6) and therefore the spectral energy density is predicted well. The difference between the total velocity variance determined from the computed and measured time series at the bar crest is for the larger part the result of the incorrect representation of the long wave energy. As for test 1a, this can possibly be

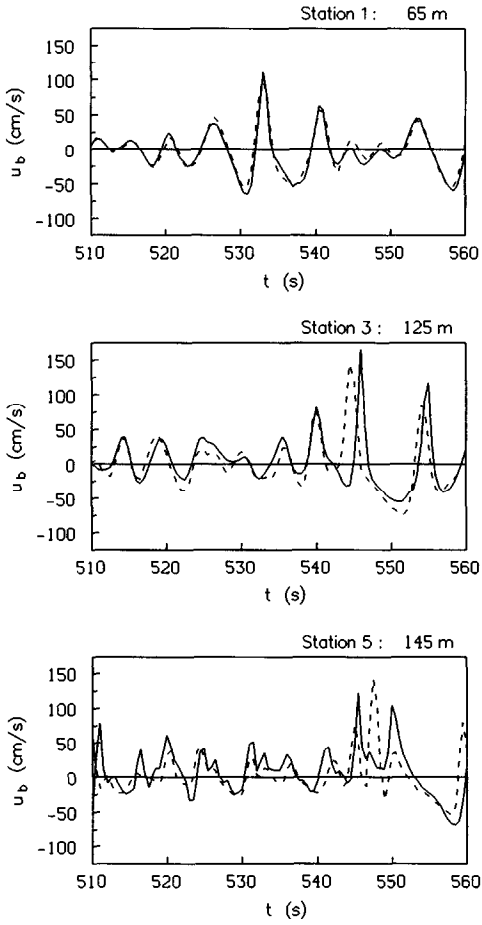

Fig. 5. Comparison of time series of the measured (solid line) and computed (dotted line) bottom velocity for experiment 1c.

ascribed to a standing wave pattern near the beach or to too strong a reduction of low-frequency energy by the breaking formulation.

It can be concluded that for test 1c the velocity skewness compares very well with the measurements. For test 1a as well as 1c, the short wave energy is predicted well by the model. The underprediction of the short wave asymmetry by the model in test 1a is therefore the result of an incorrect representation of the phases of the harmonic components. This might be partly due to the larger degree of non-linearity as compared to test 1c, such that the wave breaking already occurs at 100 m from the wave board and continues for a large propagation distance. Besides, the peak period is smaller in test 1a which decreases the accuracy of the frequency dispersion as well as the validity of the assumption of slowly-varying complex amplitudes underlying the evolution equations. The latter two effects will be explained in the following.

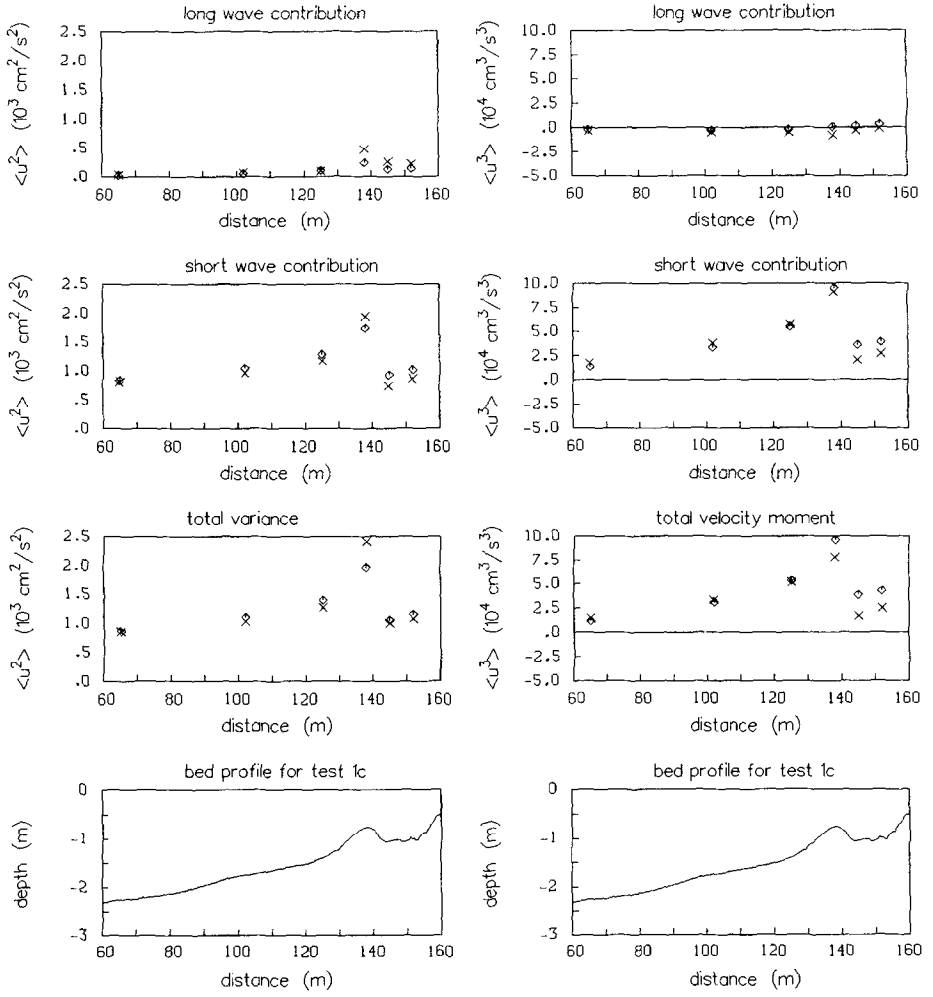

Fig. 6. Comparison of measured (crosses) and computed (diamonds) bottom velocity variance (left) and skewness (right): long wave contribution, short wave contribution and total moment respectively; experiment 1c.

Inaccurate frequency dispersion of the Boussinesq equations for freely moving shorter wave components can partly contribute to the discrepancies between computations and measurements in test 1a. The errors in the phase celerity can be computed as

$$\frac{c_{\mathrm{Bous}} - c}{c} * 100\%,$$

where c is the exact linear phase velocity and c_{Bous} is the phase velocity corresponding to the Boussinesq equations with improved frequency dispersion. For the second and

Table 2
Percent errors in the phase velocity for the second and third harmonic

	$h = 4.1$ m		$h = 1.8$ m	
	$f = 2f_p$	$f = 3f_p$	$f = 2f_p$	$f = 3f_p$
Test 1a	2.0	16	0.1	1.7
Test 1c	0.04	1.1	0.01	0.1

third harmonic these percent errors are listed in Table 2 with values for kh corresponding to a water depth of 4.1 m (at the upwave boundary) as well as a water depth of 1.8 m (at 100 m). From Table 2, it can be seen that as a result of the smaller peak period T_p, the errors in experiment 1a are considerably larger than in experiment 1c, especially for the third harmonic. The phase errors originate for the most part in deeper water close to the wave board and become significant for larger propagation distances.

Besides, the underestimation of the crest values could possibly originate from the transformation of the time–domain equations into the frequency domain; Madsen and Sørensen (1993) already pointed out that the frequency–domain model yields lower crest values than its time–domain counterpart. They did not give an explanation for this discrepancy.

The underestimation of the crest values might be due to the violation of the assumption of slowly-varying complex amplitudes $A_p(x)$ which underlies the procedure to obtain the spectral equations. The rate at which the complex amplitudes $A_p(x)$ vary in both tests can be quantified by computing the ratio of recurrence length L_r to the wave length of the first harmonic L_1. Due to the interplay between the free and bound second harmonic, the second harmonic amplitude is periodic with the recurrence length L_r. The recurrence length L_r can be expressed as (see e.g., Hulsbergen (1974) or Dingemans (1994, 1997))

$$L_r = \frac{2\pi}{k_2 - 2k_1} = \frac{c_1}{c_1 - c_2} L_2,$$

where $k_1 = \omega/c_1$ and $k_2 = 2\omega/c_2$ are the wave numbers pertaining to the free first and second harmonics respectively. The amplitudes $A_p(x)$ can be said to be slowly varying if the ratio L_r/L_1 is sufficiently large. For both tests, the ratio L_r/L_1 is computed at both the upwave boundary (at 20 m) and at 100 m. The wave length of the second harmonic L_2 is computed from linear theory, while the wave length of the first harmonic L_1 is computed using $c^2 = g(h + \zeta)$ in order to account for amplitude

Table 3
Ratio L_r/L_1 of recurrence length to first harmonic wave length

	$h = 4.1$ m	$h = 1.8$ m
Test 1a	0.7	1.2
Test 1c	2.0	2.9

dispersion. At both 20 m and 100 m, ζ was chosen as $\zeta = H_{m0}/2 = 0.45$ m for experiment 1a and $\zeta = H_{m0}/2 = 0.3$ m for experiment 1c (see Roelvink and Reniers, 1995). The results are listed in Table 3, showing that in both tests the values of L_r/L_1 are not large, as assumed. Nevertheless, this ratio is a factor 2 smaller in test 1a than in 1c, which means that the assumption of slow variation is more strongly violated in test 1a than in test 1c. This difference between experiment 1a and 1c might explain the underestimation of the short wave asymmetry and, consequently, of the velocity skewness found in experiment 1a.

4. Summary and concluding remarks

The modelling of horizontal velocities in the near-bed zone in (partially) breaking waves using a frequency–domain Boussinesq model has been studied. The near-bed velocities were obtained from the depth-averaged velocity by imposing a parabolic profile. The model has been applied to tests of irregular (partially) breaking waves on a beach.

The computation of the bottom velocities from the surface elevation yields results with an accuracy comparable to the accuracy of the predicted surface elevations. The velocity variance is predicted fairly well. For the wave test with the longer wave period, the velocity skewness is predicted well by the model. The shorter wave test however, shows an underestimation of the velocity skewness due to an underestimation of the crest values of the highest waves.

This underestimation of the crest values was seen to be the result of an inaccurate representation of the phases of the higher harmonics. It was argued that both the water-depth restriction of the Boussinesq equations and the assumption of slowly-varying amplitudes may contribute to these discrepancies. Additional research is relevant in order to determine whether the discrepancies result from the water-depth restrictions of the Boussinesq equations or from additional assumptions made in the derivation of the evolution equations underlying the present model. Further, attention should be paid to the inclusion of higher-order derivatives in the spectral evolution equations and the mean velocity in the velocity computations.

Acknowledgements

This work was started as part of the MAST-2 G8 Coastal Morphodynamics Research Program and finalized as part of the MAST-3 SAFE project. It was funded jointly by Delft Hydraulics, Delft University of Technology and the Commission of the European Communities, Directorate General for Science, Research and Development under contract No. MAS2-CT92-0027 and MAS3-CT95-0004, respectively. The laboratory data used was obtained during experiments in the framework of the "Access to Large-scale Facilities and Installations Programme" (LIP), which were funded by the Commission of the European Communities, Directorate General for Science, Research and Development under contract No. GE1*-CT91-0032 (HSMU).

References

Arcilla, A.S., Roelvink, J.A., O'Connor, B.A., Reniers, A., Jimenez, J.A., 1994. The Delta Flume '93 Experiment. Proc. Coastal Dynamics Conf., UPC, Barcelona, Feb. 1994, pp. 488–502.

Bailard, J.A., 1981. An energetics total load sediment transport model for a plane sloping beach. J. Geophys. Res. 86 (C11), 10938–10954.

Battjes, J.A., Janssen, J.P.F.M., 1978. Energy loss and set-up due to breaking of random waves. Proc. 16th Int. Conf. Coastal Eng, ASCE, New York, pp. 569–587.

Battjes, J.A., Eldeberky, Y., Won, Y.S., 1993. Spectral Boussinesq modelling of breaking waves, in: Magoon, O.T., Hemsley, J.M. (Eds.), Ocean Wave Measurement and Analysis, ASCE, New York, pp. 813–820.

Beji, S., Battjes, J.A., 1994. Numerical simulation of nonlinear wave propagation over a bar. Coastal Eng. 23, 1–16.

Bosboom, J., Klopman, G., Roelvink, J.A., Battjes, J.A., 1996. Wave kinematics computations using Boussinesq models, Proc. 25th Int. Conf. Coastal Eng., ASCE, New York, pp. 109–122.

Brocchini, M., Drago, M., Iovenitti, L., 1992. The modelling of short waves in shallow waters, Comparison of numerical methods based on Boussinesq and Serre equations, Proc. 23rd Int. Conf. Coastal Eng., vol. 4, ASCE, New York, pp. 76–88.

Deigaard, R., 1989. Mathematical modelling of Waves in the Surf Zone. Prog. Report 69, ISVA, Technical University of Denmark, Lyngby, pp. 47–59.

Dingemans, M.W., 1994. Water Wave Propagation Over Uneven Bottoms, Ph.D. Thesis, Delft University of Technology, November 1994, 780 pp.

Dingemans, M.W., 1997. Water Wave Propagation Over Uneven Bottoms, World Scientific, Singapore, 967 pp.

Eldeberky, Y., Battjes, J.A., 1996. Spectral modelling of wave breaking: Application to Boussinesq equations. J. Geophys. Res. 101 (C1), 1253–1264.

Elgar, S., Guza, R.T., 1985. Shoaling gravity waves: comparisons between field observations, linear theory, and a non-linear model. J. Fluid Mech. 158, 47–70.

Elgar, S., Guza, R.T., 1986. Non-linear model predictions of bispectra of shoaling surface gravity waves. J. Fluid Mech. 167, 1–18.

Elgar, S., Freilich, M.H., Guza, R.T., 1990. Model-data comparisons of moments of non-breaking shoaling surface gravity waves. J. Geophys. Res. 95, 16055–16065.

Freilich, M.H., Guza, R.T., 1984. Nonlinear effects on shoaling surface gravity waves. Philos. Trans. R. Soc. London A 311, 1–41.

Freilich, M.H., Guza, R.T., Elgar, S., 1990. Observations of nonlinear effects in directional spectra of shoaling gravity waves. J. Geophys. Res. 95, 9645–9656.

Hulsbergen, C.H., 1974. Origin, effect and suppression of secondary waves, Proc. 14th Int. Conf. Coastal Eng., ASCE, New York, pp. 392–411.

Madsen, P.A., Sørensen, O.R., 1992. A new form of the Boussinesq equations with improved linear dispersion characteristics. Part 2: A slowly-varying bathymetry. Coastal Eng. 18, 183–204.

Madsen, P.A., Sørensen, O.R., 1993. Bound waves and triad interactions in shallow water. Ocean Eng. 20 (4), 359–388.

Madsen, P.A., Murray, R., Sørensen, O.R., 1991. A new form of the Boussinesq equations with improved linear dispersion characteristics. Coastal Eng. 15, 371–388.

Nwogu, O., 1993. An alternative form of the Boussinesq equations for modelling the propagation of waves from deep to shallow water. J. Waterway, Port, Coastal Ocean Eng. 119 (6), 618–638.

Quinn, P.A., Petti, M., Drago, M., Greated, C.A., 1994. Velocity field measurements and theoretical comparisons for non-linear waves on mild slopes, Proc. 24th Int. Conf. Coastal Eng., ASCE, New York, pp. 540–552. 1994.

Roelvink, J.A., Reniers, A.J.H.M., 1995. LIP 11D Delta Flume experiments, Delft Hydraulics, Report H2130.

Roelvink, J.A., Stive, M.J.F., 1989. Bar-generating cross-shore flow mechanisms on a beach. J. Geophys. Res. 94 (C4), 4785–4800.

Schäffer, H.A., Madsen, P.A., Deigaard, R., 1993. A Boussinesq model for waves breaking in shallow water. Coastal Eng. 20, 185–202.

Schröter, A., 1995. Nichtlineare zeitdiskrete Seegangssimulation im flachen und tieferen Wasser. Institut für Strömungsmechanik und Elektron. Rechnen im Bauwesen, Universität Hannover, Bericht Nr. 42/1995.

Thornton, E.B., Guza, R.T., 1983. Transformation of wave height distribution. J. Geophys. Res. 88 (C10), 5925–5938.

Witting, J.M., 1984. A unified model for the evolution of nonlinear water waves. J. Comp. Phys. 56, 203–236.